Cumulative fatigue damage in low cycle fatigue and gigacycle fatigue for low carbon–manganese steel

Zhi Yong Huang, Danièle Wagner, Claude Bathias, Jean Louis Chaboche

Cumulative fatigue damage in low cycle fatigue and gigacycle fatigue for low carbon–manganese steel

Zhi Yong Huang [a,b,*], Danièle Wagner [b], Claude Bathias [b,**], Jean Louis Chaboche [c]

[a] Nanjing University of Aeronautics and Astronautics, 29, YuDao Street, 210016 Nanjing, China
[b] Université ParisOuest Nanterre La Défense, 50, Rue de Sèvres, 92410 Ville d'Avray, France
[c] O.N.E.R.A, 29, av. de la Division Leclerc, 92320 Châtillon, France

Keywords:
Low cycle fatigue
Very high cycle fatigue
Cumulative fatigue
Fatigue damage

A B S T R A C T

Typical tee and pipe components are subjected to thermal and mechanical loading histories which are variable and divided into two different regimes: low cycle fatigue and high cycle fatigue in steam generator vessel of nuclear power plants.

Carbon–manganese steel A42 are often used in such applications. In order to investigate the cumulative damage of low cycle fatigue and gigacycle fatigue, the gigacycle tests have been executed after LCF fatigue cycles damaged. The comparison of VHCF and cumulative fatigue test results shows that LCF load influences the VHCF strength.

Continuum Damage Mechanics model is employed to estimate the fatigue damage of LCF and is extended to VHCF regime. The VHCF damage is obtained from varying test resonance frequency of specimen. Moreover, the effect of LCF load on VHCF is studied by an improved cumulative damage model.

1. Introduction

Some cases of PWR components are submitted to LCF and high cycle thermal fatigue damage induced by mixing of cold and hot fluids [1]. The fatigue damage observed in PWR components is caused by thermal stratification in secondary ferritic feedwater lines. Fatigue cracks may be also observed in other component such as RHRS and RIS. LCF loads are induced by stratification of cold and hot water in horizontal parts of the feedwater line and HCF or VHCF loads are due to mixing of cold and hot water in the tee connection between auxiliary feedwater system and main feedwater line.

Damage in metals is a mainly process of the initiation and growth of micro cracks and cavities. For the sake of the complexity of microscopic defects, it is very difficult to individually and specially investigate the influence of microscopic defects on the fatigue damage of a material.

Quantitative description of damage in low cycle fatigue and high cycle fatigue, for predicting the performance of engineering structure, is possible based on results of fatigue tests. Palmgren Miner linear accumulation rule is an engineering practice standard [2], but many experimental results found its deviation from reality. Continuum Damage Mechanics (CDM) has provided an efficient non-linear cumulative damage rule proposed by Kachanov [3] and Rabotnov [4], and later developed by Lemaitre [5] and Chaboche [6] to high temperature application including creep oxidation fatigue non-linear interaction effects. Chaudonneret [7] developed it to multiaxial loading.

The purpose of this work is to obtain the LCF and VHCF fatigue behaviors and the influence of LCF damage to the gigacycle fatigue for low carbon–manganese steel. The fatigue tests are used to investigate behavior of C–Mn steels for LCF, VHCF and cumulative fatigue in ambient temperature. LCF and VHCF tests are performed in conventional hydraulic fatigue test machine and gigacycle fatigue machine [7], respectively. The cumulative fatigue tests are planed to conduct firstly LCF loading followed by VHCF loading. After given mechanical character and chemical composition of the material, experimental procedures, as well as the test results in Sections 2 and 3, a CDM methodology is applied in Section 4 in order to evaluate the damage from the variation of effective stress during LCF and VHCF fatigue tests. Moreover, an improved non-linear fatigue damage accumulation model is applied,

Abbreviations: LCF, low cycle fatigue; VHCF, very high cycle fatigue; CDM, Continuum Damage Mechanics.

* Corresponding author at: Université ParisOuest Nanterre La Défense, 50, Rue de Sèvres, 92410 Ville d'Avray, France.
** Corresponding author. Tel.: +33 1 4027 23 22.
E-mail addresses: zhiyong.huang@u-paris10.fr (Z. Yong Huang), daniele.wagner@u-paris10.fr (D. Wagner), claude@bathias.com (C. Bathias), jean-louis.chaboche@onera.fr (J. Louis Chaboche).

Nomenclature

ε_p	plastic strain	L_1, L_2, R_1, R_2	dimensions of specimen
ε_{dia}	diameter deformation	ρ	volumic mass
v_p	plastic Poisson coefficient	E_d	dynamic elastic modulus before test
E	Young modulus	f	vibration frequency
v_e	elastic Poisson coefficient	$\widetilde{E}_d$	current dynamic elastic modulus
σ	longitudinal stress	N	number of fatigue cycles
ε	longitudinal total strain	N_f	number of fatigue failure cycles
σ_M^*	maximum stress at stabilized cycle	σ_{l_0}	fatigue strength at 10^9 or 10^{10} cycles
σ_M	current maximum stress at each cycle after stabilization	σ_a	stress amplitude
D	damage parameter	σ_U	fracture stress in static tension
x	longitudinal coordinate in the symmetry axis of specimen	β, M	coefficients of Wöehler curve
		$\beta_i, \gamma_i, \zeta_i, \theta_i$	coefficients of extended Chaboche model
A_0	displacement amplitude of VHCF test		

showing its capability to describe the damage in tests, and to predict the remaining VHCF fatigue lives after prior LCF loading.

2. Material and specimen

The material is a kind of C–Mn steel of French standard NFA 36205 grade A42 which are received as 40 mm thick plates. The chemical compositions and mechanical character of material are given in Tables 1 and 2. The plates were submitted to a prior normalization thermal treatment consisting of austenitizing at 870 °C followed by air cooling, thus leading to a microstructure composed of banded ferrite and pearlite.

3. Fatigue tests

3.1. Low cycle fatigue tests

The specimen made of A42 C–Mn steels were tested under uniaxial constant strain amplitude controlled strain ratio was then approximately $R = -1$. The Instron 8500 fatigue machine is employed to perform the LCF tests.

Table 1
Chemical composition of A48 and A42 steels, wt.% (balance Fe).

Steel	C	N	S	P	Si	Mn	Al	O
A42	0.140	0.0082	0.0057	0.016	0.225	0.989	0.045	0.0049

Table 2
Material character of A42 and A48.

Type of steel	Elastic modulus E (Gpa)	Volumic mass ρ (kg/m^3)	UTS (MPa) (20 °C)	Poisson coefficient
A42	209	7850	460	0.3

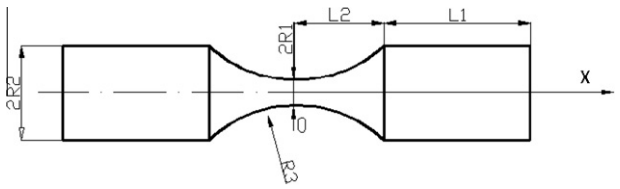

Fig. 1. Specimen of gigacycle fatigue and cumulative fatigue ($R_1 = 3.25$, $R_2 = 6.35$, $R_3 = 38$, $L_1 = 31.47$).

On account of the particularity of gigacycle fatigue, a resonance state requests a certain form and dimensions as Fig. 1 shows. Obviously, its form only permits the LCF test controlled under transverse diameter deformation. The variation of the diameter deformation should be converted to longitudinal direction through the formulas below [8]:

$$\varepsilon_p = -\frac{1}{v_p}\left(\varepsilon_{dia} + v_e \cdot \frac{\sigma}{E}\right) \tag{1}$$

$$\varepsilon = \frac{\sigma}{E}\left(1 - \frac{v_e}{v_p}\right) - \frac{1}{v_p}\varepsilon_{dia} \tag{2}$$

where ε_{dia}, ε_p, ε are diameter deformation, longitudinal plastic strain, longitudinal total strain, respectively. E, v_e are Young modulus, elastic Poisson coefficient. v_p is plastic Poisson coefficient and its value is always 0.5. σ is the longitudinal stress.

In all LCF tests, reversed triangle strain waveform was submitted to the specimens. The failure condition is set as its maximum stress decreasing 20% after its cyclic saturation. The Fig. 2 shows the LCF test results (red[1] empty square points).

The stress evolution of strain controlled tests is not keeping constant because of cyclic isotropy hardening or softening and deterioration of material with the progressive fatigue cycles. The cyclic saturation stress in cyclic stabilization stage is regarded as the equivalent stress amplitude for LCF. The relationship between strain amplitude and equivalent stress amplitude in LCF for A42 is shown in Fig. 3. The equivalent stress amplitude versus number of cycles is presented in Fig. 5 with red square points.

3.2. Very high cycle fatigue tests

The ultrasonic fatigue testing method brought advantages of effectiveness and economy characters comparing with conventional tests method. Quite a lot of very high cycle fatigue investigations [9] on the metallic materials have discovered that the fatigue failure may happen in gigacycle fatigue regime with the stress amplitude being well below the traditional fatigue limit of the classical Wöhler S–N curve.

The ultrasonic fatigue test machine must include some basic components as Fig. 4 shown [16]. An ultrasonic generator which provides a sinusoidal signal with 20 kHz; a piezoelectric converter excited by the generator which transforms the electrical signal into longitudinal mechanical vibration with same frequency; a horn that amplifies the vibration displacement in order to obtain the required strain amplitude in the middle section of specimen; a

[1] For interpretation of color in Figs. 2, 3, and 5–12, the reader is referred to the web version of this article.

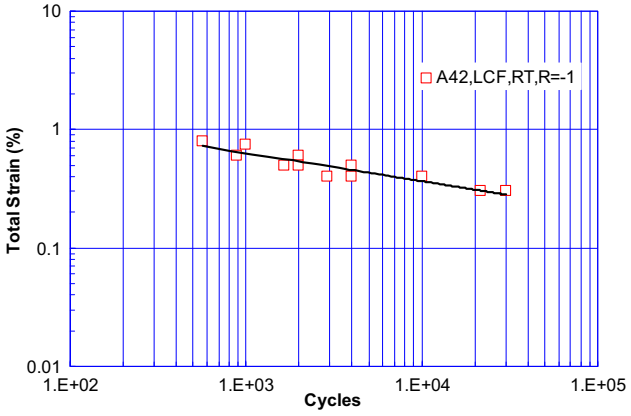

Fig. 2. A42 LCF test results.

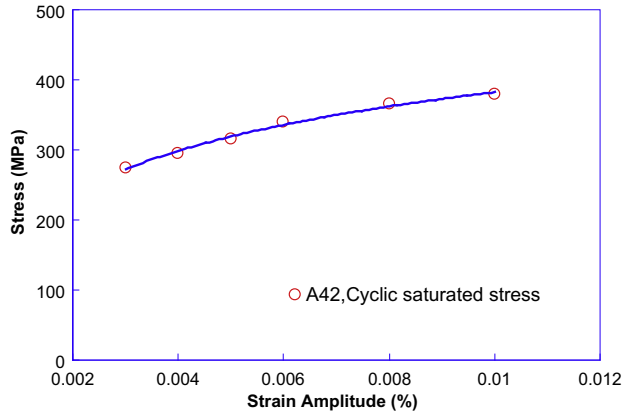

Fig. 3. The cyclic curve: stress amplitude as a function of strain amplitude.

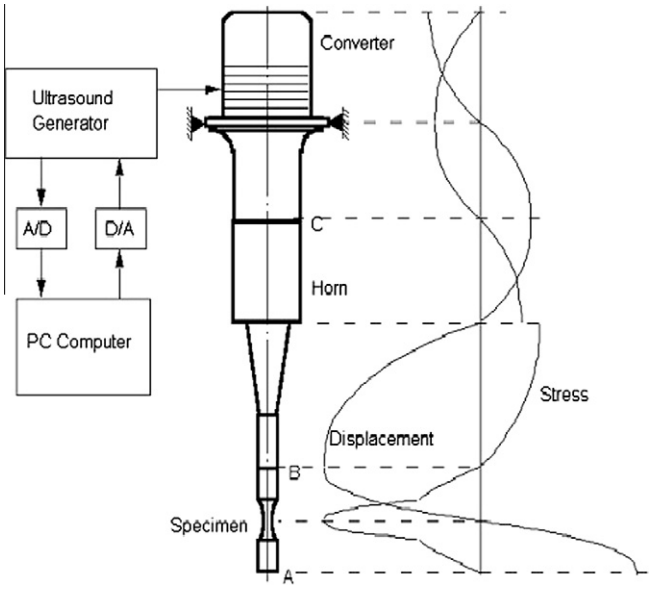

Fig. 4. The schematic diagram of ultrasonic fatigue test system.

computer control system is necessary to control the load amplitude and acquire test data. The converter, horn and specimen form a mechanical vibration system which includes four stress nodes (null stress; A–C in Fig. 4) and three displacements nodes (null displacement) for an intrinsic frequency of 20 kHz. The specimen works in the resonance vibration state and its center is a displacement node with maximum stress amplitude. In addition to this, compressed air cooling gun is necessary to be used to prevent the temperature increasing of specimen in the tests.

The gigacycle fatigue tests for A42 steel employed the ultrasonic fatigue devices (20 kHz) in order to study VHCF damage behavior at $R = -1$ and room temperature. The results are plotted by red round points in Fig. 5.

3.3. Prior monotonic tension effect to VHCF

When loading a low carbon steel like C–Mn steel A42, there is a point on the stress–strain curve where the yield point drops as strain increases called Lüders phenomenon [10]. The yield stress decreases from the upper yield value to the lower yield value, and the strain (displacement) continues to increase while the stress stays roughly constant (actually there can be a little fluctuation) (Fig. 6). Five percent monotonic tensile deformation is over Lüders strain and increases yield strength of the material.

Specimens of A42 pretreated 5% monotonic tensile deformation are immediately tested in gigacycle test system. Due to the cold hardening effect, VHCF strength is improved about 20 MPa (Fig. 7).

3.4. Cumulative damage fatigue tests

In order to investigate the preloaded effect of LCF on behavior of VHCF for A42 steel, three specimens are submitted to a same prior 0.34% strain amplitude (strain ratio: -1) LCF loading but different number of cycles 10, 50, 100, respectively. The subsequent VHCF tests are performed with 200 MPa stress amplitude at $R = -1$, room temperature. Compared with no damaged VHCF test results, no observable damage appears in Fig. 8.

We increased the prior LCF strain amplitude to 0.62% with a number of cycles fixed at 100. The test results are shown in Fig. 9, where the VHCF fatigue strength presents a significant decrease.

4. The damage of LCF and VHCF

4.1. Fatigue damage measurement

4.1.1. LCF damage measurement

In LCF tests, the cyclic stress after saturation is used to describe the damage evolution on the strain behavior. In the beginning of LCF test, the hardening or softening of cyclic stress before saturation at strain amplitude, which is depending on material, is not considered as a damage growth [12], but the accumulated micro plastic deformation with reversible travel of dislocation. A damaged material contains micro cracks from defects that reduce the load carrying capacity. Therefore, the further change of cyclic stress after saturation is an indicator of damage growth. The effective stress concept is proposed by Rabotnov [4] to describe the effect of damage on the strain behavior. The damage parameter D is defined as follows:

$$D = 1 - \frac{\sigma_M}{\sigma_M^*} \tag{3}$$

σ_M^* is the maximum stress at stabilized cycle. σ_M is the current maximum stress at each cycle after fatigue cyclic saturation.

Damages curves defined by Eq. (3) from maximum stress evolution, for LCF with 0.8% and 0.6% strain amplitudes, are plotted with red square and triangle symbols, respectively, in Fig. 11.

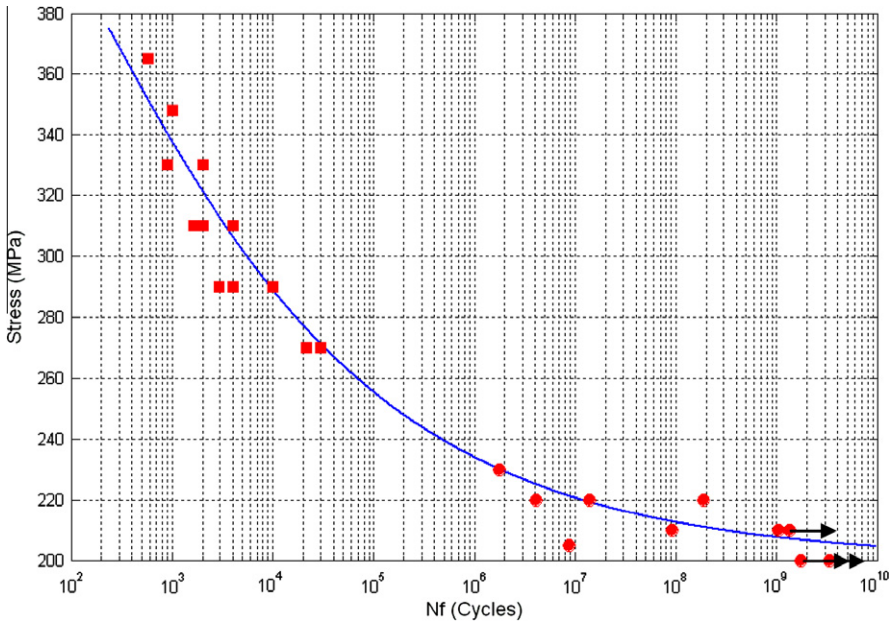

Fig. 5. LCF and VHCF test results (red square points for LCF, red round points for VHCF, blue curve for Chaboche *S–N* model).

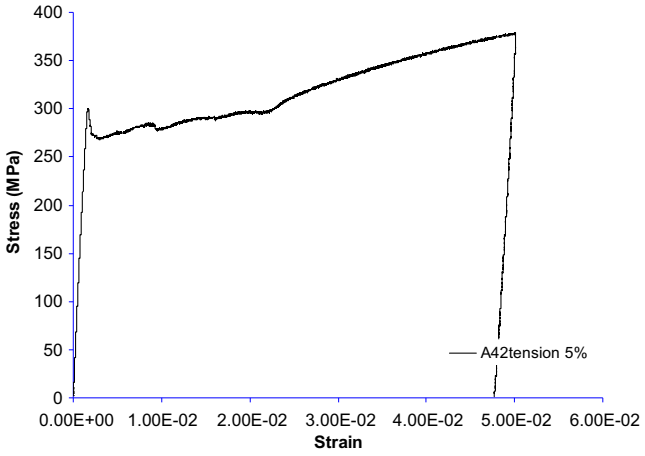

Fig. 6. A42 monotonic tension test (5% deformation).

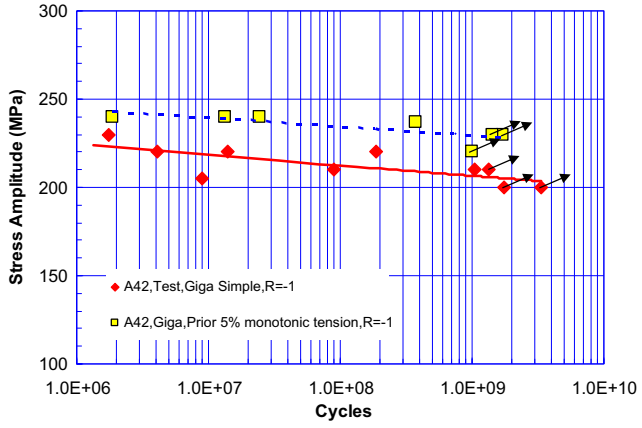

Fig. 7. A42 gigacycle test results with and without prior monotonic tension 5%.

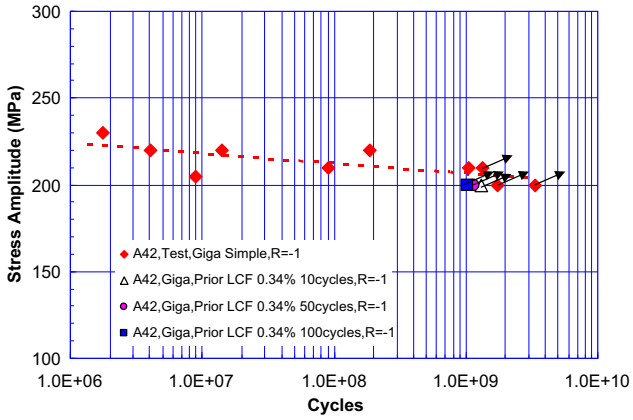

Fig. 8. A42 gigacycle test results with and without prior LCF load (0.34% strain amplitude, 10 cycles triangle point, 50 cycles diamond point, 100 cycles blue square point).

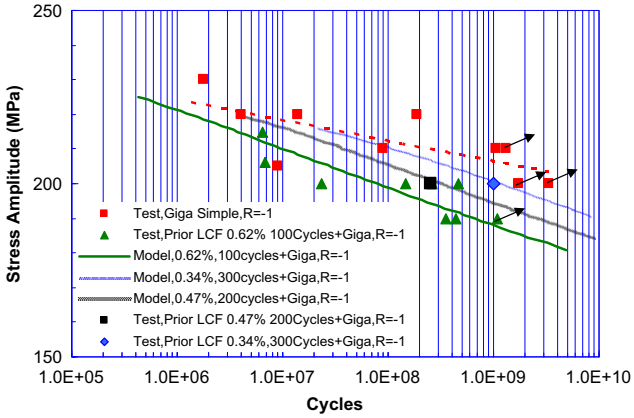

Fig. 9. A42 cumulative fatigue test (prior 0.62% strain amplitude, 100 cycles damaged following VHCF) results and extended Chaboche approach (green real line).

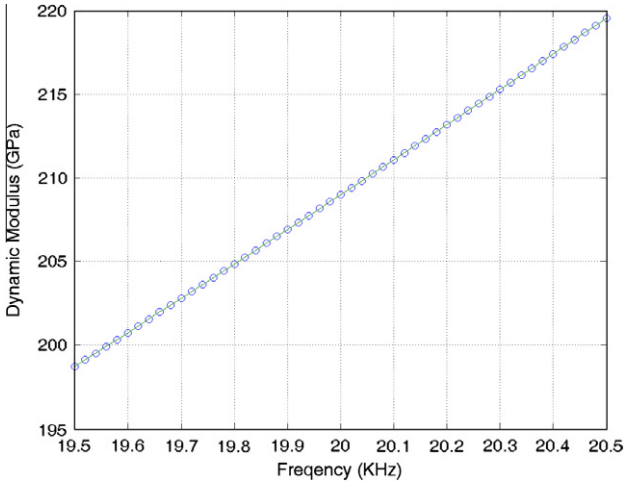

Fig. 10. The linear relationship between frequency and dynamic modulus in VHCF.

4.1.2. VHCF damage measurement

The gigacycle tests are controlled by displacement through the piezoelectric fatigue machine working at 20 kHz. If the specimen is in resonance state, in the reduced section part of specimen, displacement amplitude distribution solution is [9]:

$$U(x) = A_0\varphi(L_1, L_2)\frac{\sinh(\beta x)}{\cosh(\alpha x)}, \quad |x| \leqslant L_2 \tag{4}$$

where

$$\varphi(L_1, L_2) = \frac{\cos(kL_1)\cosh(\alpha L_2)}{\sinh(\beta L_2)} \tag{5}$$

where

$$\omega = 2\pi f, \quad k = \frac{\omega}{C}, \quad C = \sqrt{\frac{E_d}{\rho}}, \quad \alpha = \frac{1}{L_2}\operatorname{arccosh}\left(\frac{R_2}{R_1}\right),$$

$$\beta = \sqrt{\alpha^2 - k^2}.$$

x is longitudinal coordinate along with the symmetry axis of specimen as shown in Fig. 1. A_0 is the displacement amplitude, L_1, L_2, R_1, R_2 are the dimensions of specimen as shown in Fig. 1.

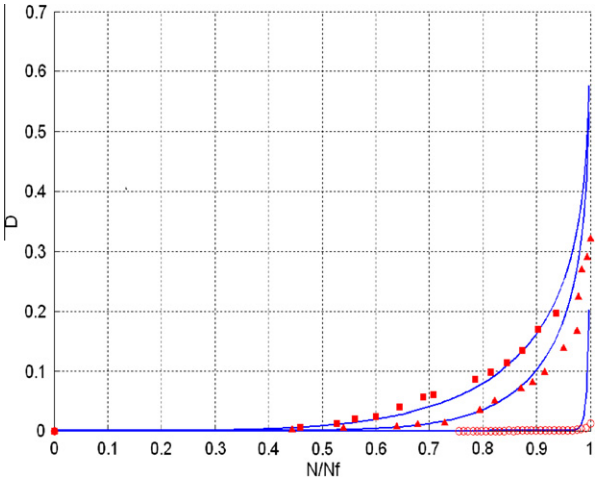

Fig. 11. The damage evolution for A42 in LCF and VHCF test (red square or triangle points are from LCF tests; red round empty points from VHCF tests; blue curves are the estimation).

ρ, E_d are the density and dynamic elastic modulus, respectively. f is the specimen vibration frequency.

The strain amplitude distribution in specimen reduced part is:

$$\varepsilon(x) = \frac{dU(x)}{dx}, \quad |x| \leqslant L_2 \tag{6}$$

And stress amplitude distribution is:

$$\sigma(x) = E_d\varepsilon(x), \quad |x| \leqslant L_2 \tag{7}$$

At the smallest section of specimen, $x = 0$ (Fig. 1), the strain and stress reach their maximum. The piezoelectric ceramic is driven by a signal generator and makes the specimen vibrating at constant displacement amplitude before failure; we suppose that strain amplitude keeps a constant value during the VHCF test. The cyclic stress amplitude is variable because the dynamic elastic modulus decreases due to VHCF fatigue damaged. So, the damage definition from effective stress for VHCF is as follows,

$$D = 1 - \frac{\sigma_M}{\sigma_M^*} = 1 - \frac{\widetilde{E}_d}{E_d} \tag{8}$$

where $\widetilde{E}_d$ would be the current dynamic elastic modulus during the damage evolution. The gigacycle machine works at 20 kHz with a ±500 Hz frequency tolerance and can detect specimen resonance frequency automatically from the power generator.

The specimen design Eq. (9) is used to calculate the cylinder part length of specimen to fit the resonance vibration [9]. The two independent variables: f resonance frequency and E_d dynamic elastic modulus are variable during the test.

$$L_1 = \frac{1}{k}\arctan\left\{\frac{1}{k}[\beta\coth(\beta L_2) - \alpha\tanh(\alpha L_2)]\right\} \tag{9}$$

In the Eq. (9), the R_1, R_2, L_2, L_1 are the specimen dimensions as shown in Fig. 1. The varying dynamic elastic modulus affects its resonance frequency during the gigacycle fatigue. We apply the resonance frequency to obtain the cyclic elastic modulus and to estimate the gigacycle fatigue damage. The linear relationship between resonance frequency and elastic modulus of specimen is presented in Fig. 9 by employing trial calculation to expression (9). The program is that we firstly suppose a tentative frequency between 19.5 kHz and 20.5 kHz (the tolerance resonance frequency of the gigacycle fatigue test system) and increase the dynamic modulus with step of 0.01 GPa to recalculate the trial length L_1'. When the difference of L_1' and L_1 (the real length) is less than 10^{-9} (the convergence condition), the dynamic elastic modulus is accepted at the frequency. We loop the calculation at different frequency and the relationship of resonance frequencies and elastic modulus can be obtained (Fig. 10).

The VHCF damage defined by Eq. (8) and obtained from the variation of test resonance frequency is plotted in Fig. 11 with 210 MPa stress amplitude ($R = -1$, room temperature) in empty red round points. As expected for HCF or VHCF conditions, the damage detection is very late.

4.2. Chaboche S–N model and damage model

Using the one-dimensional damage differential model, valid for reversed conditions (no mean stress) [5]:

$$\frac{dD}{dN} = \left[1 - (1-D)^{\beta+1}\right]^{\alpha(\sigma_a)}\left[\frac{\sigma_a - \sigma_{l_0}}{M(1-D)}\right]^{\beta} \tag{10}$$

The number of cycles until failed under constant amplitude loading σ_a as:

$$N_f = \frac{1}{(\beta+1)[1-\alpha(\sigma_a)]}\left(\frac{\sigma_a - \sigma_{l_0}}{M}\right)^{-\beta} \tag{11}$$

The damage can be written with the variable N/N_f:

$$D = 1 - \left[1 - \left(\frac{N}{N_f}\right)^{\frac{1}{1-\alpha}}\right]^{\frac{1}{\beta+1}} \tag{12}$$

where

$$\alpha(\sigma_a) = 1 - a\left\langle\frac{\sigma_a - \sigma_{l_0}}{\sigma_U - \sigma_a}\right\rangle \tag{13}$$

The equation can be rewritten as:

$$N_f = (\sigma_U - \sigma_a)\left(\frac{\sigma_a - \sigma_{l_0}}{B}\right)^{-\beta-1} \quad \text{with} \quad B = \left(\frac{\sigma_{l_0}}{a(\beta+1)}M^{\beta}\right)^{1/\beta+1} \tag{14}$$

where σ_{l_0} is the fatigue strength at 10^9 or 10^{10} cycles. Parameters $B = 200$, $\beta = 3.5$, $\sigma_{l0} = 202$ MPa are identified by S–N curve (Fig. 5). Parameter $a = 0.14$ is identified by the damage results as points shown in Fig. 11. The additive parameter is static fracture stress $\sigma_U = 500$ MPa.

4.3. Two stress level cumulative damage model for LCF and VHCF

The prior LCF cyclic load followed by a VHCF cyclic load is a very extreme test for a material which is simplified from practice complex loadings of nuclear pipes. Chaboche's two level cumulative damage model [14] is extended to LCF and VHCF regimes here.

$$\frac{dD}{dN} = \frac{D^{\zeta}}{(1-\zeta)N_f(\sigma_a)} = \frac{D^{\zeta}}{N_f^*(\sigma_a)} \tag{15}$$

Eq. (15) first part is used for loads above the fatigue limit which normally recognizes the fatigue strength at 10^7, the second one for those below. The $N_f(\sigma_a)$ is the function chosen for the S–N curve, taken as a power function. σ_a could be equivalent stress amplitude in LCF, HCF or VHCF regime at $R = -1$. One group of parameters of Basquin's model is very hard to describe three regimes fatigue damage cumulative behavior, such as the S–N curve is steeper in LCF regime but more flat and never approaching horizontal asymptote in VHCF regime. In order to describe S–N curve at different regimes like LCF, HCF and VHCF, the multi group parameters of Basquin [13] model are applied for S–N curve $N_f(\sigma_{a_{eff}})$ and hidden function $N_f^*(\sigma_{a_{eff}})$ [14].

$$N_{fi}(\sigma_{ia}) = \left(\frac{\sigma_{ia}}{M_i}\right)^{-\gamma_i} \tag{16}$$

$$N_{fi}^*(\sigma_{ia}) = \left(\frac{\sigma_{ia}}{M_i^*}\right)^{-\beta_i^*} \quad (i = 1,\ 2,\ 3) \tag{17}$$

where $\beta_i^* = \theta_i\gamma_i$, θ_1, θ_3 ($i = 1, 2, 3$) are the additional parameters. Subscript $i = 1, 2, 3$ expresses LCF, HCF and VHCF regime, respectively. If the cumulative test is only in HCF regime with two different stress levels, the S–N curve function and hidden function $N_{fi}^*(\sigma_{ia})$ are degraded to Chaboche fatigue multilevel damage accumulation model where parameters M_i^* never play role in the results for multilevel fatigue tests in one regime.

Equality of both sides of (15) automatically gives the function ζ:

$$1 - \zeta = \frac{N_f^*(\sigma_a)}{N_f(\sigma_a)} \tag{18}$$

If the test has two level loads, the fatigue life at second level in the case of VHCF cyclic loading, we have $i = 3$.

$$\frac{n_3}{N_{f_3}} = 1 - \left(\frac{n_1}{N_{f_1}}\right)^{\frac{1-\zeta_3}{1-\zeta_1}} \tag{19}$$

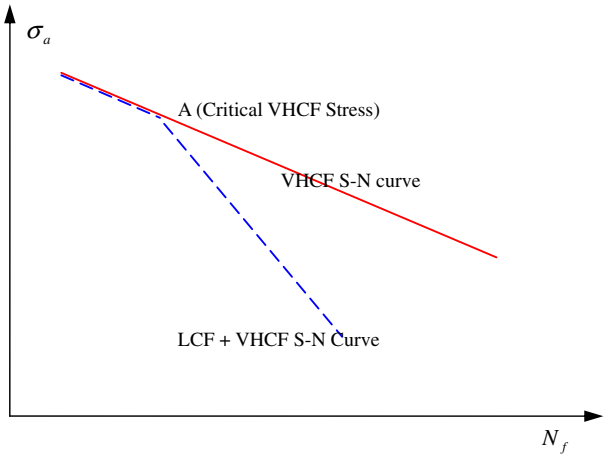

Fig. 12. The schematic S–N curve of LCF and VHCF.

where ζ_1 and ζ_3 are values of the function ζ at the two levels,

$$\frac{1-\zeta_3}{1-\zeta_1} = \frac{N_{f_1}}{N_{f_3}}\frac{N_{f_3}^*}{N_{f_1}^*} \tag{20}$$

The model parameters θ_1, θ_3 are taken here as 0.1 and 0.5 to estimate the VHCF test results under preloaded with 0.62% strain amplitude with 100 cycles. In Fig. 9, the green continuous line calculated by the model is in good agreement with the experimental results. Moreover, the load level and number of cycles of LCF play in right direction that higher prior LCF load results in greater reduction for subsequent VHCF strength, as shown by black and blue lines on Fig. 9, respectively, for 0.47%, 200 cycles and 0.34%, 300 cycles.

From the previous test results (Fig. 9), the LCF load damaging VHCF strength lies on its strain amplitude and number of cycles (strain ratio: -1) which reflected in our model is the position of inflexion point A (Fig. 12) called critical VHCF stress, under which the damage effect of LCF appears, and degree slope of following S–N curve, as illustrated schematically by the blue broken line in Fig. 12.

In the extended Chaboche cumulative model for LCF and VHCF, θ_1, θ_3 are necessary parameters. Factor θ_1 changes position of the critical VHCF stress (A in Fig. 12) on the non damaged VHCF S–N curve. In other words, θ_1 adjusts inflexion point A going up or down along the red line (Fig. 12). In addition, parameter θ_3 influences the curve slope below point A (Fig. 12, blue discontinuous line).

5. Conclusion

The article first investigated the low carbon–manganese steel LCF and VHCF behavior, respectively. Then, cumulative fatigue damage tests, with first LCF level followed by VHCF loading have been executed. Fatigue damage models based on CDM are applied to describe the LCF, VHCF damage evolution and their cumulative fatigue behavior. The conclusions are listed as follows:

1. Prior monotonic plastic deformation (5%) increases the fatigue strength in VHCF, but LCF loading is deleterious for VHCF. The test results show that after 100 cycles with 0.62% strain amplitude loading the damaging effect for VHCF strength is very significant.
2. The Chaboche damage model is applied to LCF by introducing the effective stress concept and extended to VHCF regime through damage definition from the variation of measured E_d. This damage model can describe the damage behavior in LCF and VHCF.

3. The extended two level fatigue damage model proposed here is in good agreement with the LCF and VHCF cumulative fatigue tests and correctly predicts that higher prior LCF loading results in more reduction in VHCF fatigue strength.

Acknowledgements

The authors would like to acknowledge AREVA for support of this work. Mr. Y. Meyzaud, Mr. P. Joly and Mr. J.A. Leduff are thanked for their help to the work.

Reference

[1] Le Duff AJ, Lehéricy Y, Lefrançois A, Mendez J. Effects of surface finish and LCF pre-damage on the HCF endurance limits of A 304L austenitic stainless steel. Deutscher Verband fur Materialforschung und prufung e.V. 2009:1023–33.
[2] Miner MA. Cumulative damage in fatigue. J Appl Mech 1945;67:A159–64.
[3] Kachanov ML. Time of the rupture process under creep conditions. TVZ Akad Nauk SSR Otd Tech Nauk 1958;8:26–31.
[4] Rabotnov YN. Creep problems in structural members. North Holland Publishing Comp; 1969.
[5] Lemaitre J, Chaboche JL. Mechanics of solid materials. Cambridge: Cambridge University Press; 1990. p. 344–44.
[6] Chaboche JL. Continuum damage mechanics present state and future trends. Nucl Eng Des 1987;105:19–33.
[7] Cailletaud G, Chaboche JL. Lifetime predictions in 304 S.S. by damage approach. In: Conf ASME Pressure Vessel and Piping Division, Orlando; 1982.
[8] Lieurade HP. Comportement mécanique et métallurgique des aciers dans le domaine de la fatigue oligocyclique – Etude des phénomènes et application à la croissance des fissure. Thèse 1978:173–4.
[9] Bathias C, Paris PC. Gigacycle fatigue in mechanical practice. New York: Marcel Dekker; 2005. p. 11–48.
[10] Verel DJ, Sleeswyk AW. Luders band propagation at low velocities. Acta Metall 1973;21:1087–98.
[12] Chaboche JL. Continuous damage mechanics – a tool to describe phenomena before crack initiation. Nucl Eng Des 1981;64:233–47.
[13] Basquin OH. The exponential law of endurance tests. In: Proc of the American society for testing and material, vol. 10; 1910. p. 625–30.
[14] Chaboche LJ, Kaminski M, Kanoute P. Extension and application of a non-linear fatigue damage accumulation rule for variable amplitude loading programs. Deutscher Verband fur Materialforschung und prufung e.V. 2009:627–39.
[16] Bathias C. Piezoelectric fatigue testing machines and devices. Int J Fatigue 2006;28:1438–45.

Further reading

[11] Bathias C, Drouillac L, Le François P. How and why the fatigue *S–N* curve does not approach a horizontal asymptote. Int J Fatigue 2001;23:143–51.
[15] Lemaitre J. Coupled elasto-plasticity and damage constitutive equations. Comput Methods Appl Mech Eng 1985;5:131–49.
[17] Huang ZY, Du WW, Wagner D, Bathias C. Relation between the mechanical behavior of a high strength steel and the microstructure in gigacycle fatigue. Mat Sci Forum 2010;636–637:1459–67.
[18] Kueppers M, Sonsino CM. Assessment of the fatigue behavior of welded aluminium joints under multiaxial spectrum loading by a critical plane approach. Int J Fatigue 2006;28:540–6.
[19] Miner MA. Cumulative damage in fatigue. J Appl Mech 1945;67:71–82.
[20] Chaudonneret M. A simple and efficient multiaxial fatigue damage model for engineering applications of macro-crack initiation. J Eng Mater Technol 1993;115:373–9.